Numerical investigation of the effect of ultrasound on paper drying

MUNEVVER ELIF ASAR, ZAHRA NOORI, AND JAMAL YAGOOBI

ABSTRACT: The paper drying process is very energy inefficient. More than two-thirds of the total energy used in a paper machine is for drying paper. Novel drying technologies, such as ultrasound (US) drying, can be assessed numerically for developing next-generation drying technologies for the paper industry.

This work numerically illustrates the impact on drying process energy efficiency of US transducers installed on a two-tiered dryer section of a paper machine. Piezoelectric transducers generate ultrasound waves, and liquid water mist can be ejected from the porous media. The drying rate of handsheet paper in the presence of direct-contact US is measured experimentally, and the resultant correlation is included in the theoretical model.

The drying section of a paper machine is simulated by a theoretical drying model. In the model, three scenarios are considered. In the first scenario, the US modules are positioned in the dryer pockets, while in the second scenario, they are placed upstream of the drying section right after the press section. The third case is the combination of the first and second scenarios. The average moisture content and temperature during drying, enhancement of total mass flux leaving the paper by the US mechanism, total energy consumption, and thermal effect of heated US transducers are analyzed for all cases. Results show that the application of the US can decrease the total number of dryer drums for drying paper. This numerical study is based on the US correlation obtained with the US transducer in direct contact with the paper sample. Thus, future work should include US correlation based on a non-contact US transducer.

Application: In this paper, for the first time, the effect of the application of a US mechanism in a multi-cylinder dryer section is numerically investigated. The results of this study aim to uncover the potential impact of US drying on a paper machine.

Approximately 420 million metric tons of paper were manufactured worldwide in 2018 [1]. Even with modern technologies, papermaking involves an immensely energy-intensive drying operation, which has a great economic significance and contributes to climate change [2]. The energy consumed during the paper drying process corresponds to around 70% of the energy used in papermaking, or by a paper machine [1]. According to the U.S. Department of Energy's report published in 2015 [3], the use of novel drying technologies in paper drying can save 64 trillion Btu annually across the nation's pulp and paper industry. Thus, the effect of enhancing the paper dewatering methods is crucial.

Approximately 90% of paper produced is dried by multi-cylinder dryers [4,5], consisting of 20–120 dryer drums. Paper gets dried by traveling through heated and rotating cast-iron cylinders. Generally, the dryer drums are internally heated by condensing steam, which transfers heat mainly through the conduction mode of heat transfer. Paper entering the drying section has a dry-basis moisture content in the range of 0.82–1.86 after being pressed in the pressing section [6]. Linerboard paper is the most produced paper type in the United States, corresponding to almost one-third of the produced paper in the United States in 2010 [3]. Linerboards are widely used to manufacture corrugated boxes [3]. Therefore, this study focuses on the drying of linerboard paper.

Various researchers studied heat and mass transfer in porous media and paper drying. Nissan and Hansen [7] were one of the first who simulated paper drying, and they divided a dryer drum into four phases, with each phase having a set of boundary conditions. Yagoobi et al. [8] simulated free-water removal during paper drying. That study simultaneously solved transient energy and mass conservation equations in the thickness direction of the paper, considering water vapor fluxes by diffusion and liquid water fluxes by convection. Later, Asensio and Seyed-Yagoobi [9] improved the model by adding the impact of porosity and thickness changes during drying and used better contact conductance correlations between paper and dryer drum surface. Seyed-Yagoobi et al. [10] combined a gas-fired infrared emitter with multiple dryer drums for various grades of paper. They stated that the model was giving [9] predicted experimental data from pilot machine trials very well. Using the same model, paper drying with single and two-tiered dryer configurations was studied numerically, and no significant differences were found between them [11]. In addition, Hoshi et al. [12] demonstrated a transient 1D drying model for paper, placed in between a hot dryer roll and a canvas. This study modeled the water inside and outside the cell membranes of the wood fiber and treated vapor movement by diffusion and advection and liquid water movement by capillary forces. Similarly, Lu and Shen's model [6] considered convection and capillary transport for liquid fluxes and convection and diffusion transport for water vapor and air fluxes. They verified the model against the data obtained from a working paper machine. Furthermore, Sadeghi and Douglas [13] provided a validated paper drying simulator for cylinder dryers, impingement air dryers, and hybrid dryer configurations for the full range of paper grades. Asensio et al. [14] compared three different paper drying models. A review of main paper drying models can be found in Sadeghi [15]. Overall, most drying models utilize the volume-averaging approach detailed by Whitaker [16]. Few studies [9-11,17-19] have incorporated paper's structural changes during drying into their model, since porosity and thickness changes affect the temperature, moisture variation, and liquid and vapor fluxes during drying.

Wet samples can be dried by ultrasonic waves when the sample is in direct contact or in proximity with an ultrasound-emitting piezoelectric transducer. Piezoelectric transducers generate ultrasound by efficiently converting electric energy to mechanical vibrations. This vibrational energy induces instabilities on the liquid-air interface, and consequently, liquid water mist can be ejected from the porous media [20]. The porous media dries as water mist leaves the boundaries due to the applied ultrasound. In a recent study, Zhang and Abatzoglou [21] extensively reviewed fundamentals, applications, and potentials of ultrasound-assisted drying. They discussed the various ultrasonic phenomena, such as the sponge effect, acoustic streaming, local oscillations, atomization, and thermal effect. These phenomena can enhance mass and heat transfer in the drying of porous media. This study also mentioned the effect of ultrasound on drying efficiency. Furthermore, Peng et al. [20] experimentally investigated the ultrasonic drying of fabrics, using piezoelectric crystal and mesh-type transducers. They verified the capillary wave theory with their data on the atomization of droplets. They reported that the ultrasound-assisted drying process is composed of two modes: water atomization and thermal evaporation. The characterization of these modes depends on the transducer, fabric type, and operating conditions. Patel et al. [22] utilized multiple ultrasonic transducers for fabric drying experiments, and they concluded that ultrasound performed better at higher initial moisture contents for a given applied power. Dupuis et al. [23] studied direct-contact ultrasonic drying with fabrics and presented their non-dimensional equation for ultrasonic dewatering that depended on the surface area of the cloth and transducer acceleration.

Ultrasound-assisted drying can be considered as a novel drying technology for the pulp and paper industry. Thus far, ultrasound (US) drying has mainly been studied for fabric and food products. Therefore, there is a need for studies focusing on the application of the US mechanism within the drying section of a paper machine. In this paper, for the first time, the effect of the application of a US mechanism in a multi-cylinder dryer section is numerically investigated. The results of this study aim to uncover the potential impact of US drying on a paper machine where a direct-contact US correlation is used as a starting point. Direct-contact US results will pave the way for the fundamental understanding of the US mechanism.

THEORETICAL MODEL

The drying section of a papermaking machine is simulated by a theoretical drying model, developed by Asensio and Seyed-Yagoobi [9] for simulating conventional steam-heated, multi-cylinder drying of paper. The model predicts moisture and temperature profiles inside the paper and describes uncoated paper in a two-tiered dryer configuration, as shown in **Fig. 1** (without the US modules). The model is transient and one-dimensional in space (in thickness). Changes in porosity and paper shrinkage due to moisture and temperature variations during drying were considered as described by Asensio and Seyed-Yagoobi [9]. The effect of ultrasound on paper drying was captured by altering the original boundary conditions provided by Asensio and Seyed-Yagoobi [9]. Mass and energy conservation are the governing equations of the model where heat flux, liquid flux, and vapor flux are calculated by Fourier's, Darcy's, and Fick's Laws. For the complete set of governing equations and boundary conditions, one can consult Asensio and Seyed-Yagoobi [9] to fully understand the current study's modeling. The capillary pressure correlation of linerboard [24] is used in the model instead of using a correlation for wood in the original model. A list of the terminology referenced in the following sections is given in the Appendix.

Boundary conditions

Nissan and Kaye [25] divided cylinder drying into four phases, according to the location of interest on a dryer drum. Four drying phases can be seen in Fig. 1. The model developed by Asensio and Seyed-Yagoobi [9] utilizes this four-phase model, which is described as follows.

In Phase I, the bottom surface of the paper sheet is in contact with the dryer surface, and the top surface of the paper sheet is open to ambient air and thus permits evaporation from the top surface. In Phase II, the bottom surface is in contact with the dryer surface. However, the top surface is in contact with felt (porous sheet) rather than being open to ambient air without any restriction, as compared to Phase I. Phase III is similar to Phase I. In Phase IV, the paper travels between two dryer drums and is not in contact with any surface on either top or bottom. Evaporation can occur from both sides of the paper. When paper travels from the beginning of Phase I to the end of Phase IV for a given drum, it completes its residence time for that dryer

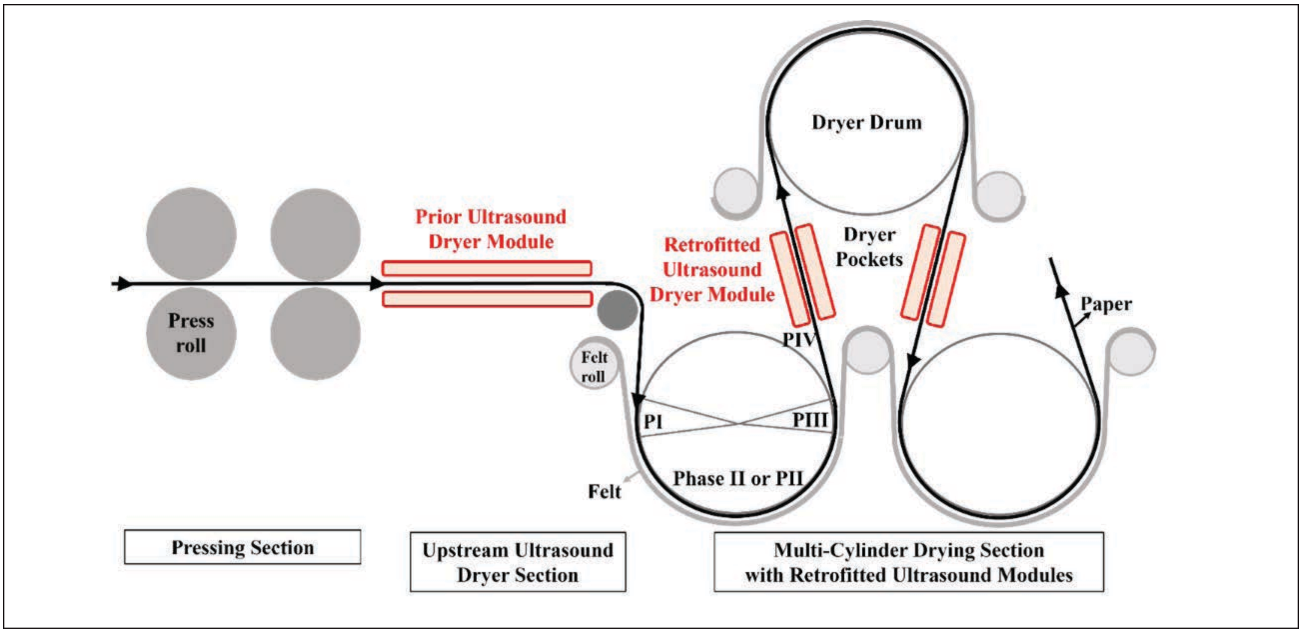

1. Press and dryer section with addition of prior and retrofitted ultrasound (US) dryer modules (in red), along with nomenclature for the four phases of drying.

and moves to another dryer drum until it is dry. Note that top (z=Z) and bottom (z=0) nodes were not located at the physical boundaries; instead, they were located a half-step size into the paper. This approach was also used in the original model by Asensio and Seyed-Yagoobi to simplify the numerical model and is acceptable for small step sizes in thickness direction [9]. This numerical study placed ultrasound modules in the middle half of Phase IV and just before the drying section. If an ultrasound module exists at a location between the dryers or before the drying section, the boundary conditions at that location need to be altered. Here, the effect of ultrasound on the drying mechanism was studied by adding a liquid flux term to the boundary condition equations. This is needed because the water mist generated by the US is in liquid form. Physically, the ejected mist has to leave the porous media from the open boundaries. Enforcing liquid flux at the open boundaries (when the US is applied) will ensure that the liquid mist leaves the paper. Note that the liquid flux at the boundaries not only affects the boundary nodes but also affects the temperature, saturation, moisture content, liquid, and vapor fluxes of the interior nodes as well. This additional liquid flux ($J_{w,o}$), was determined experimentally and described in the "Methodology" section. By utilizing $J_{w,o}$, mass and energy boundary conditions at the bottom boundary (z=0) in Phase IV are updated, as shown in Eq. 1 and Eq. 2. The effect of US can be seen by the second term on the right hand side in Eq. 1 and the fifth term on the right hand side in Eq. 2. The enthalpy for liquid water (H_w) was used in the energy boundary condition when representing the energy leaving the porous media due to the exiting mist.

$$\frac{\partial M}{\partial t} = \frac{1}{\Delta z}(-J_{w,i} - J_{w,o} - J_{v,i} - J_{v,o}) \tag{1}$$

$$\left(c_w \rho_w s \varepsilon + c_f \rho_f (1-\varepsilon)\right)\frac{\partial T}{\partial t} = \frac{1}{\Delta z}\left(k_{eff}\frac{\partial T}{\partial z} - J_{v,i}H_v - J_{w,i}H_w - J_{v,o}H_v - J_{w,o}H_w - h(T - T_a)\right) \tag{2}$$

Similarly, with the presence of ultrasound, the boundary conditions for Phase IV at the top boundary (z=Z) should be updated and are:

$$\frac{\partial M}{\partial t} = \frac{1}{\Delta z}(+J_{w,i} - J_{w,o} + J_{v,i} - J_{v,o}) \tag{3}$$

$$\left(c_w \rho_w s \varepsilon + c_f \rho_f (1-\varepsilon)\right)\frac{\partial T}{\partial t} = \frac{1}{\Delta z}\left(-k_{eff}\frac{\partial T}{\partial z} + J_{v,i}H_v + J_{w,i}H_w - J_{v,o}H_v - J_{w,o}H_w - h(T - T_a)\right) \tag{4}$$

Drying performance during the prior US modules is found using the same governing equations and boundary conditions described above, corresponding to the modified Phase IV boundary condition. In other words, in the prior US section, the length of the phases I, II, and III is zero because there is no dryer drum in the prior US section. The paper experiences the boundary conditions corresponding to the modified Phase IV while passing through the prior US section. Also, to better compare with the baseline case, $J_{v,o}$ term is considered zero at both boundaries while paper

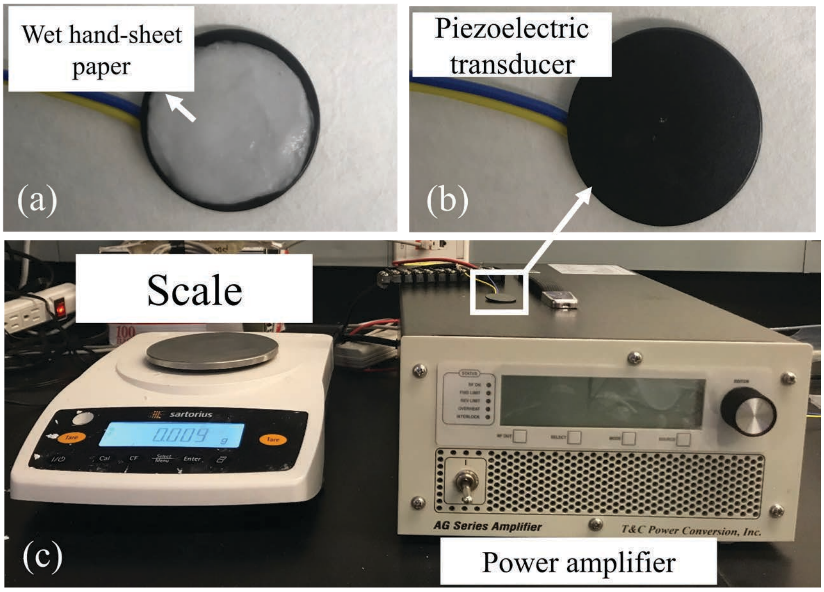

2. Experimental setup for direct-contact US drying experiments: (a) wet handsheet paper on the transducer, (b) a piezoelectric transducer; and (c) the overall setup, including a scale, a power amplifier, and a transducer.

passes through prior US modules. In addition, the temperature of the surrounding air during the prior US section is assumed to be equal to the temperature of the sheet exiting the pressing section. This is an acceptable assumption, because no heat is applied during the prior US section.

METHODOLOGY

Experimental US drying rate correlation

An experimental US drying rate correlation is input into the theoretical drying model to assess the performance of US modules installed on a paper drying machine. This section discusses how this experimental drying rate correlation was obtained. **Figure 2** shows the major components of the experimental setup for direct-contact ultrasound-assisted drying where the fresh 2-cm diameter handsheet papers were used. The preparation of the samples follows TAPPI Standard Test Method “Forming handsheets for physical tests of pulp (Reaffirmation of T 205 sp-02),” and the pressed handsheets have an initial dry basis moisture content (DBMC) of 1.49. Note that there was a slight difference from TAPPI Standard T 205 sp-02 in the final size of the paper. To achieve the smaller paper sizes, short cylindrical molds (with internal diameter=2 cm) were placed before fully opening the sheet maker cylinder’s gates very fast (the last step of the sheet-making process according to TAPPI Standard T 205 sp-02 before couching and pressing). The ultrasound drying experiments are conducted at 3W of load power and 1.7 MHz frequency, which corresponds to the manufacturer-specified resonance frequency of the transducer. The sample’s top surface is open to the ambient air during the experiments, whereas the bottom surface is in direct contact with the transducer. However, this contact ceased shortly, at every 10 s, when the sample was brought to the scale for weight measurement. The effect of this loss of contact on the drying performance is ignored. The ambient is a standard laboratory environment at ~19°C (with ~50% relative humidity). The experiments are repeated ten times, averages are taken, and the maximum standard deviation of moisture content is within 4% over the entire drying time during the experiments.

Figure 3a represents the average DBMC, where Fig. 3b shows the corresponding drying rate with respect to drying time for conditions in **Table I**. The drying rate was estimated by taking a derivative of DBMC and multiplying it with basis weight (BW). The derivate was taken by second-order central differencing. Generally, higher moisture content levels result in higher drying rates because more water is available for the ultrasound to generate mist. Other researchers also observed similar results. Patel et al. [22] reported that ultrasound performed better at higher initial moisture contents for a given applied power. Also, the drying rate is relatively lower than the

BW	Pressing	$WBMC_{init}$	$DBMC_{init}$	s_{init}	Fiber Type	th_{fin}	Sample Area
204 g/m²	Applied	0.65	1.86	0.74	Unrefined softwood	0.6 mm	3.08 cm²

I. Parameters for handsheet papers used in the experiments. See Appendix for terms.

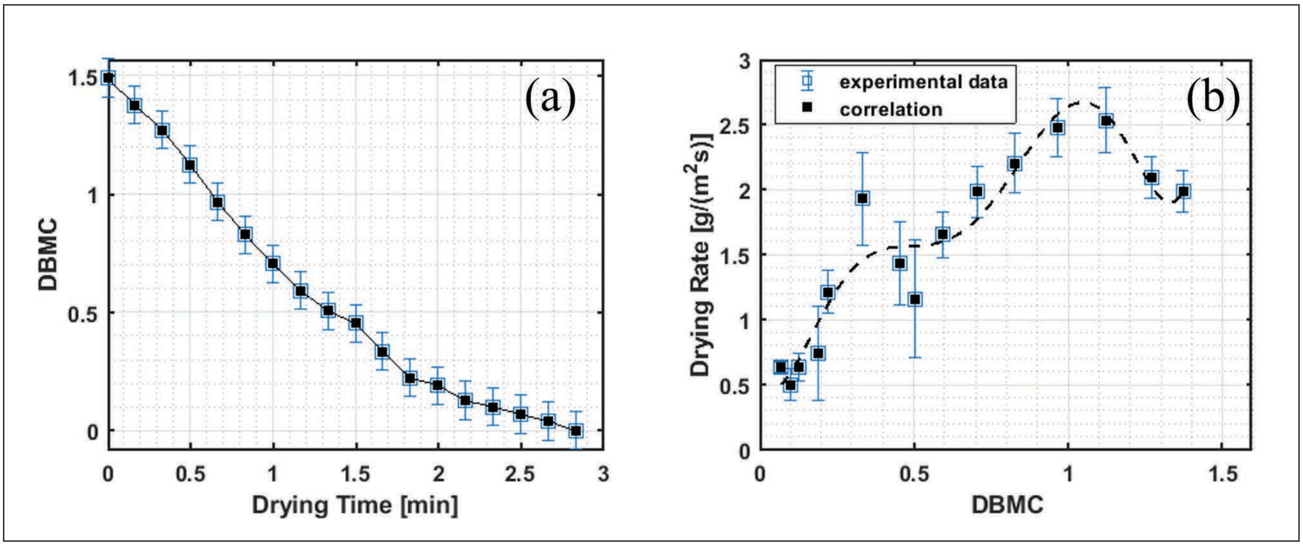

3. Experimental data showing experimental drying curve (a) and drying rate (b) of handsheet paper when in contact with the US transducer (DBMC=dry basis moisture content).

neighboring points at the beginning of drying. This corresponds to the DBMC range of 0.9–1.4. These regions can be called the combined warmup-drying zone due to the initial warm-up of the transducer (and sample) and ultrasonic misting. The increase of drying rate at the early stages of drying can be attributed to this combined warmup-drying zone. That is because the drying rate increases when the sample temperature increases due to decreasing the water viscosity and increasing the vapor saturation pressure.

A drying rate correlation can be found that is a function of the average DBMC and given in Eq. 5. This correlation is also plotted in Fig. 3b. This is the experimental US drying rate correlation (Eq. 5) that is combined with the numerical model, which is based on the combined thermal and ultrasound effects. The effect of transducer thermal load was analyzed and is given in the “Results” section. In addition, this correlation is for unrefined softwood. Thus, using refined paper may yield slightly different results due to the differences explored in Park et al. [26]. It was shown that the beating of fibers changes the fibrillation of the surface [26,27], free water/bound water regions, and freeness [26].

$$\begin{aligned} \textit{Drying Rate correlation} &= 5.87x10^{-11}(\overline{DBMC}[\%])^6 - 2.40x10^{-8}x(\overline{DBMC}[\%])^5 \\ &+ 3.62x10^{-6}x(\overline{DBMC}[\%])^4 - 0.000248x(\overline{DBMC}[\%])^3 \\ &+ 0.007x(\overline{DBMC}[\%])^2 - 0.053x(\overline{DBMC}[\%]) \\ &+ 0.585\left[\frac{kg}{m^2 s}\right], \end{aligned} \quad (5)$$

$$R^2 = 0.97 \text{ for } 0.07 \leq \overline{DBMC} \leq 1.38$$

Numerical analysis

Highly coupled governing equations and the given set of boundary conditions were solved numerically via MATLAB (Mathworks; Natick, MA, USA) using finite difference methods. For time marching, a fully explicit Euler method was used. Time-derivative terms were discretized with first-order finite differencing. The discretization of spatial derivatives was second-order differencing. The model used 12 nodes across the thickness and found a solution at every 0.25 ms to generate the mesh size and time-step size-independent solutions.

The same BW and bone-dry thickness values as the handsheet paper in the experiments were inserted into the numerical simulation. Moreover, numerical simulations were run until DBMC=0.2, because the theoretical model simulated free water removal, not bound water removal, during multi-cylinder drying. Reardon et al. [28] stated that the transition to bound water from free water happens at DBMC <~0.3, while Schennerberger et al. [29] had results of vaporization energy showing that a threshold at DBMC=0.2 is reasonable for focusing on the free water removal region.

RESULTS

The summary of the studied cases is given in **Table II**, whereas the placement of the US modules is illustrated in Fig. 1. Even though the correlation used is for the direct-contact US and the placement of the US modules may introduce some challenges, both retrofitted and prior US cases are studied to illustrate the potential impact of the application of US mechanism in a paper machine. Note that a wrap or “w” is equivalent to the total length of Phases I-IV for the selected dryer, or 5.26 m. Figure 1 shows the prior US cases as a horizontal section, but the prior US section can consist of wraps to conserve space. De-wetting of the cases is predicted for the operating conditions given in **Table III**. It is important to note that most results are based on theoretical calculations.

Cases	Description	Retrofitted US	Prior US
Baseline	Multi-cylinder dryer drums with no US modules.	No	No
R_US_all	Retrofitted US on every dryer at middle-half of every Phase IV.	Yes	No
R_US_first19	Retrofitted US at middle-half of Phase IV for the first 19 dryers.	Yes	No
P_US_10w	US modules installed prior to dryer drum section with a length of 10 wraps.	No	Yes
P_US_5w	US modules installed prior to dryer drum section with a length of 5 wraps.	No	Yes
P_US_5w + R_US_first10	US modules installed prior to dryer drum section with a length of 5 dryer wraps followed by retrofitted US at middle-half of Phase IV for the first 10 dryers.	Yes	Yes

II. Summary of cases (US = ultrasound).

Operating Conditions		Value	Unit
Paper	Basis weight, BW	204	g/m^2
	Initial dry-basis moisture content, $DBMC_{init}$	1.00	-
	Initial wet-basis moisture content, $WBMC_{init}$	0.5	-
	Initial saturation, s_{init}	0.41	-
	Bone-dry thickness, th_{final}	0.6	mm
	Fiber/cellulose density, ρ_f	1500	kg/m^3
	Initial temperature	45	°C
	Permeability	8×10^{-16}	m^2
	Specific heat	1340	J/(kgK)
Air	Temperature, T_a (dryer section)	85	°C
	Temperature, T_a (upstream of dryer section)	45	°C
	Humidity ratio	0.12	-
	Sheet speed	6.00	m/s
	Cylinder diameter	1.829	m
	Cylinder surface temperature, T_{su}	120	°C
Machine	Phase I length	0.188	m
	Phase II length	3.089	m
	Phase III length	0.188	m
	Phase IV length	1.794	m
	Length of US modules in Phase IV (if retrofitted)	0.897	m
	Felt tension	3 (17)	kN/m (pli)

III. Operating conditions for numerical simulation.

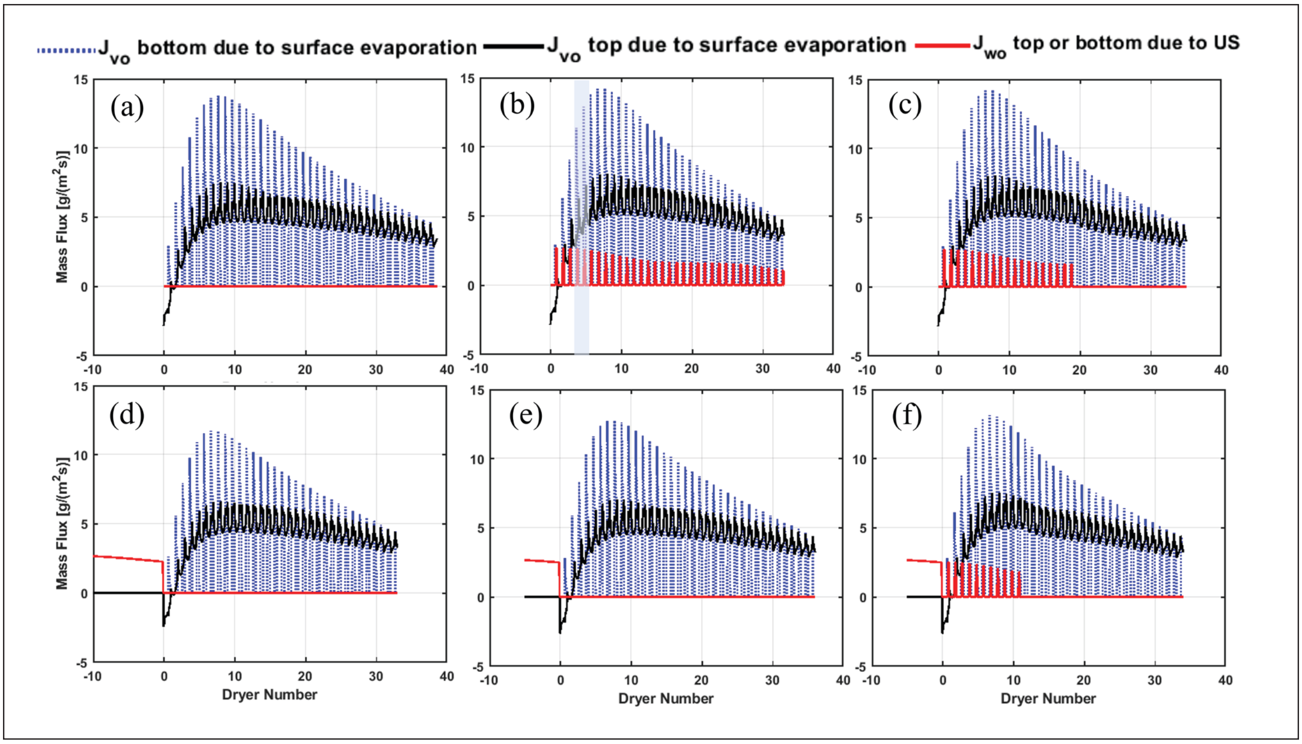

4. Numerical data comparing vapor and liquid mass fluxes that exit the paper vs. dryer number for cases: (a) baseline; (b) R_US_all; (c) R_US_first19; (d) R_US_select; (e) P_US_10w; (f) P_US_5w + R_US_first10. A zoomed version is given in Fig. 5a.

Figure 4 shows the comparisons of water vapor and liquid water fluxes exiting the paper for all the studied cases in Table II. Comparing these fluxes is critical, because the drying rates strongly depend on the mass exiting from the boundaries. The vapor flux due to evaporation ($J_{v,o}$) is illustrated for both the top (z=Z) and bottom (z=0) surfaces. The bottom surface (z=0) is always the surface on the dryer side, and the top surface (z=Z) is on the air side, although the paper flips due to the two-tiered configuration of the paper machine. When the dryer number is negative, it does not correspond to actual dryer drums, but instead, it corresponds to the prior US modules upstream of the dryer drum section. Figure 4a is for the baseline case, and liquid fluxes are zero because there is no US applied. In addition, the vapor flux exits from the bottom boundary (dryer side) are always greater than that of the top boundary (air side), because the bottom node is closer to the dryer and has higher temperatures. Both vapor fluxes increase with time/dryer number in the beginning due to increases in the sheet temperature. This is followed by a decline due to the decreased moisture availability of the surfaces. Note that, at the very early stages of drying, the vapor flux is negative because the surrounding air temperature is higher than the initial sheet temperature, and moisture in air condensates on the paper sheet. This is because the partial pressure of water vapor in ambient air is higher than the saturation pressure of water at sheet temperature when the paper sheet is relatively colder than the ambient humid air.

Figure 4b shows the mass flux comparisons for the retrofitted US case where **Fig. 5a** is a zoomed section of the shaded region of the plot shown in Fig. 4b. As seen in Fig. 4b, $J_{v,o}$ at z=0 is only non-zero when it is in Phase IV, because in other phases, the bottom surface is in contact with the dryer surface, and surface evaporation is blocked. At the beginning of Phase IV, the evaporation at z=0 is relatively high and then drops, as the surface's moisture availability decreases. On the other hand, $J_{v,o}$ at z=Z is always non-zero because the top surface allows for evaporation at all drying phases. At z=Z and in Phase II, $J_{v,o}$ values were multiplied with a factor of 0.8 due to the presence of felt, and the drop in $J_{v,o}$ can be clearly identified from Fig. 5a. Moreover, in Fig. 4b, the solid red line representing the water flux ($J_{w,o}$) due to US $J_{w,o}$ was determined using the experimental drying rate correlation, using corresponding average DBMC at a given time. From the drying rate curve, shown in Fig. 3b, the maximum $J_{w,o}$ value is about 2.5 g/(m²s), which is lower than the evaporation mass fluxes at almost all of the drying section.

For a better comparison, a comparison factor in total mass flux leaving the boundaries is plotted in Fig. 5b. The factor is denoted as C_j and shown in Eq. 6. It represents the percent ratio of total $J_{w,o}$ to $J_{v,o}$ on both sides of the paper. In other words, C_j is the moisture removal rate by liquid form divided by the moisture removal rate by the vapor form. Because $J_{w,o}$ estimation uses the averaged DBMC, the value for a given time's $J_{w,o}$ value is the same for both sides of the paper. Therefore, the numerator in

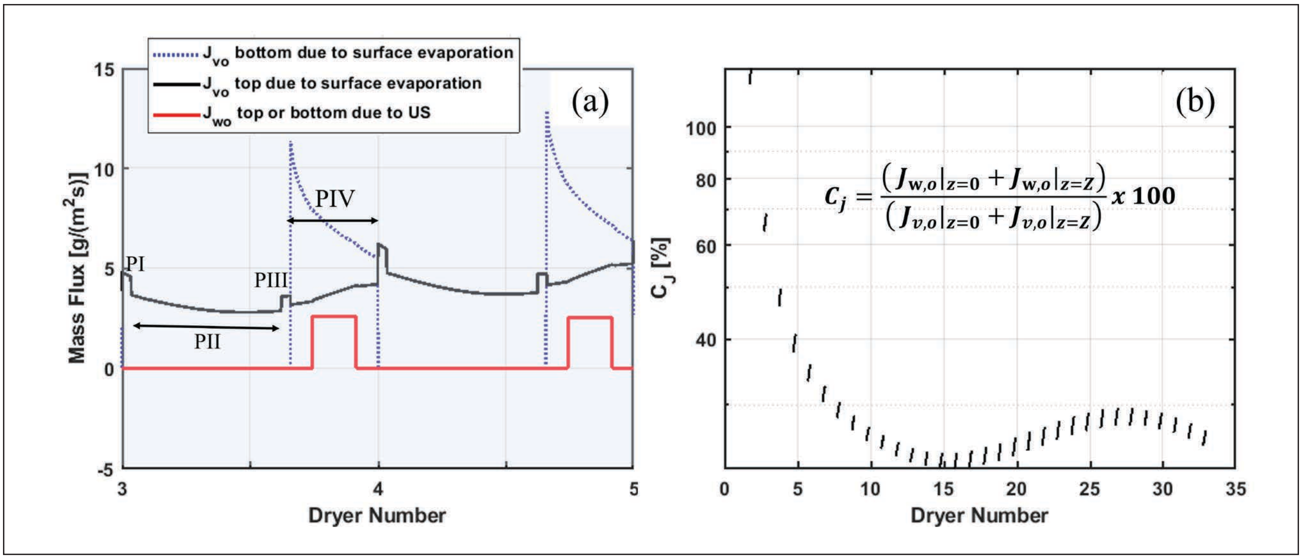

5. Numerical data showing vapor and liquid mass flux comparison vs. dryer number: (a) zoomed image for the shaded area in Fig. 4b; and (b) mass flux comparison at the boundaries for the retrofitted US case (R_US_all).

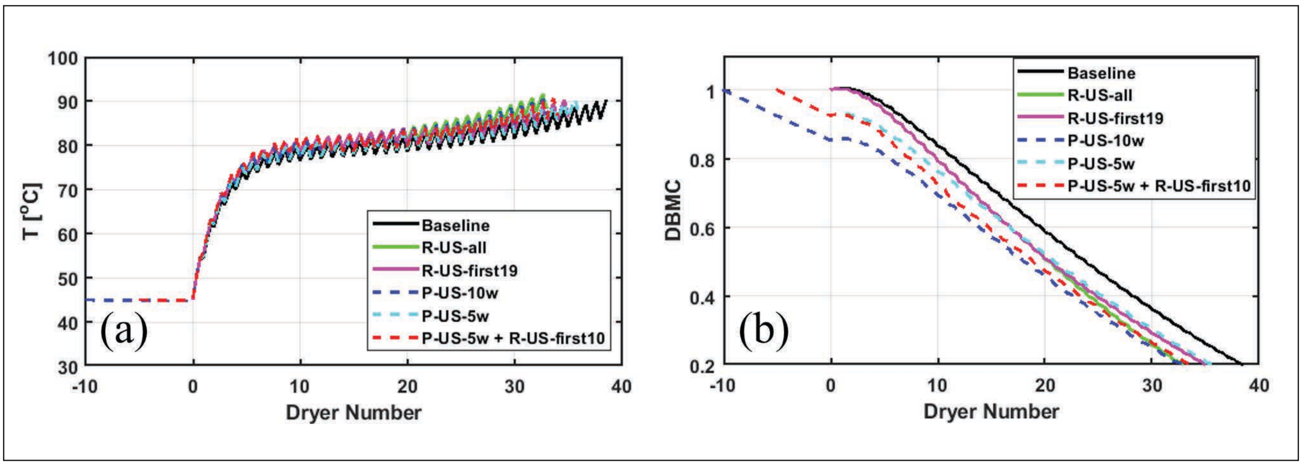

6. Numerical data: (a) average temperature, and (b) average dry-basis moisture content of paper sheet during drying.

Eq. 6 is twice that of $J_{w,o}$ to account for both sides of the paper. C_j is non-zero only when the US is applied and is remarkably high at the first couple of dryers. It starts to decay afterward as the sheet temperature is high enough to allow for much higher surface evaporation fluxes. Towards the end of the drying section, although $J_{w,o}$ is on the decline, C_j rises slightly. This increase in C_j is due to decreases in $J_{v,o}$ because of the limited moisture availability at the boundary nodes for surface evaporation. Although C_j is about 22%–30% when it is non-zero, it is zero most of the drying length because the US is applied on only the middle-half section of Phase IV. Moreover, an average comparison ratio ($\overline{C_j}$) can be calculated by Eq. 7, where t' is the time when paper reaches $\overline{DBMC}$ =0.2 and is 8.9% for R_US_all case.

$$C_j = \frac{(J_{w,o}|_{z=0} + J_{w,o}|_{z=Z})}{(J_{v,o}|_{z=0} + J_{v,o}|_{z=Z})}\ x\ 100 = \frac{2\ x\ J_{w,o}|_{z=0\ or\ Z}}{(J_{v,o}|_{z=0} + J_{v,o}|_{z=Z})}\ x\ 100 \quad (6)$$

$$\overline{C_j} = \frac{\int_{t=0}^{t'}(J_{w,o}|_{z=0} + J_{w,o}|_{z=Z})\,dt}{\int_{t=0}^{t'}(J_{v,o}|_{z=0} + J_{v,o}|_{z=Z})\,dt}\ x\ 100 \quad (7)$$

In the R_US_first19 case, US modules are only retrofitted in the first half of the paper machine. The comparison of the mass fluxes of R_US_first19 is given in Fig. 4c. As expected, after the 19th dryer, R_US_first19 has slightly different vapor flux values than R_US_all. Moreover, Fig. 4d-f demonstrates the cases with prior US modules and

Cases	Total Length of US Modules, m	Average Comparison Ratio ($\overline{C}j$), %	Decrease in Dryer Number	Decrease in Dryer Number, %	Energy Ratio
R_US_all	29.60	8.9	6	15.4	0.67
R_US_first19	17.04	5.8	4	10.3	0.69
P_US_10w	52.6	24.9	6	15.4	0.38
P_US_5w	26.3	11.3	3	7.7	0.38
P_US_5w + R_US_first10	35.27	15.6	5	12.8	0.47

IV. Summary of the results for all cases.

a prior US case when combined with the retrofitted US at the beginning of the dryer drum, respectively. As mentioned previously, surface evaporation is canceled in the model before the dryer drum section to make a fair judgment between the baseline model and the prior US cases.

Figure 6a shows the average temperature of all the cases studied. Alternating boundary conditions for different stages of drying cause fluctuating temperature curves. Sheet temperature increases when the paper is in contact with the hot dryer surface during Phases I, II, and III. On the other hand, sheet temperature reduces in Phase IV because the pocket temperature is lower than the sheet temperature, except at the first dryer drum. The decrease in temperatures during Phase IV is also a result of elevated evaporation rates, considering that both surfaces are available for surface evaporation. Furthermore, the application of the US slightly changes the paper's temperature compared to that of the baseline case. This is expected because the non-zero liquid fluxes at the boundaries not only affect parameters at the boundaries, but also change the internal dynamics of the porous medium, such as local moisture content, vapor and liquid fluxes, etc.

Figure 6b shows the average dry-basis moisture content until DBMC=0.2 for all cases. Prior US modules help to have a drier paper onset of the cylinder dryer section. For example, for P_US_10w, the DBMC of paper reduces to ~0.85 from 1.0 after the paper passes through the prior US section. In addition, for all cases, the paper's initial temperature is lower than the surrounding air temperature, and moisture condensates on relatively cold paper. This results in an increase in DBMC at the very early stages in the cylinder-dryer section. Furthermore, all US cases result in a decrease in the required number of dryers.

Decrease in required dryer numbers and total length of US modules, average comparison ratios ($\overline{C}_j$), and energy ratios are tabulated in **Table IV**. Energy ratio compares the US cases to the baseline case and is given in Eq. 8. At a given location or time (t) during the drying process, the difference between the mass of water ($\Delta\overline{M}|t$) is calculated between the baseline and US cases. The numerator of the energy ratio is the energy consumed to evaporate $\Delta\overline{M}|t$ using the dryer drums with an efficiency (η_{dryer}) of 0.65 [30,31]. Whereas the denominator corresponds to the total energy consumed by the US modules using an ultrasonic power based (P_{US}) based on the load power and ultrasonic power efficiency (η_{US}) of 0.85. (The current ultrasonic power efficiency was not optimized; however, an optimal design efficiency of ~0.85 can be readily achievable [32].) Therefore, if the energy ratio of a certain US case at the end of drying is higher than 1, that US case consumes less energy to de-wet the same amount of water than the dryer drums, and vice versa.

$$Energy\ Ratio = \frac{\frac{(\Delta\overline{M}|_t)\cdot H_{fg}}{\eta_{dryer}}}{\frac{\int_{t=0}^{t} P_{US}\,dt}{\eta_{US}}} = \frac{\frac{(\Delta\overline{DBMC}|_t\ \cdot BW)\cdot H_{fg}}{\eta_{dryer}}}{\frac{\int_{t=0}^{t} P_{US}\,dt}{\eta_{US}}} \tag{8}$$

The key findings using Table IV and Fig. 6b can be summarized as follows; however, it should be noted that these results are limited to operating conditions and the contact US correlation considered in this study.

- All US cases result in a decrease in required dryer numbers up to 15% (R_US_all and P_US_10w). This finding means that the sheet speed can be increased with the application of the US mechanism when the total number of dryers is kept constant. In other words, if a paper machine adopts US modules, the machine's throughput can be increased by applying the US mechanism.
- Retrofitted US cases can be an advantage to enhance drying, especially for dryer- or space-limited machines.
- Overall, the energy ratio for all the US cases is less than 1. This means that the US requires more energy to dry a moist paper than the baseline case. This implies that the atomization requires more power to vibrate the liquid and generate liquid mist that escapes from the paper than the baseline drying method.

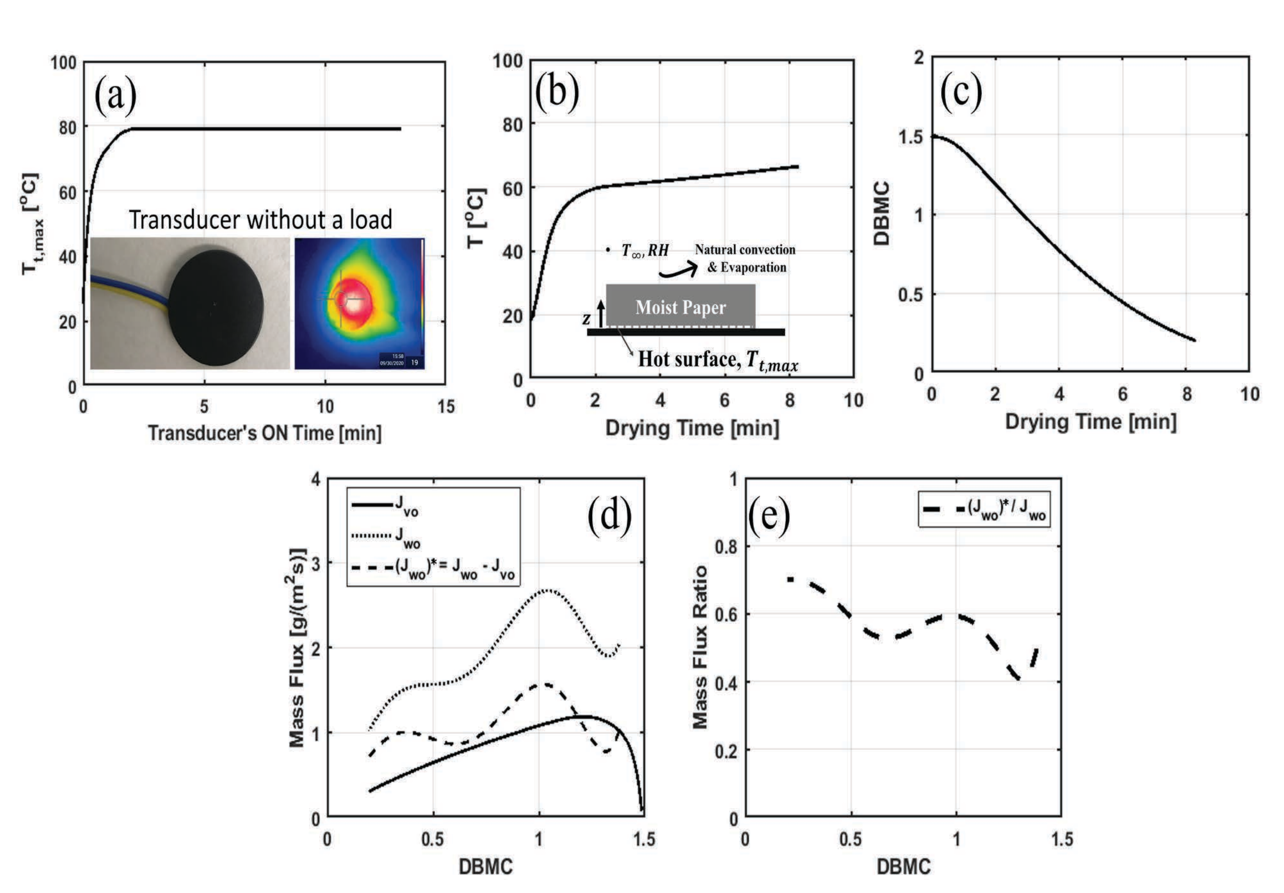

7. Experimental data (a) and numerical data (b-e): (a) maximum measured surface temperature of the transducer ($T_{t,max}$); (b) average temperature of the moist paper when it is placed on a hot surface with $T_{t,max}$; (c) drying curve of the moist sample in (b); (d) vapor flux ($J_{v,o}$) exiting the moist porous medium and liquid flux ($J_{w,o}$) and corrected liquid flux (($J_{w,o}$)*) for comparison; and (e) mass flux ratio (($J_{w,o}$)*) / $J_{w,o}$).

- R_US_all and P_US_10w result in the same decrease in dryer number, although R_US_all's US section is much shorter. This implies that P_US_10w can give an excellent headstart for drying the paper, but the great enhancement at the beginning is not carried on until the end of the dryer drum section. In addition, P_US_10w has a much lower energy ratio than R_US_all.
- Although perhaps it would practically be easier to add prior US modules to a paper machine, it will not be as effective in decreasing the required dryer number (increasing the sheet speed) while decreasing the energy consumption.
- When ten retrofitted US modules are added to P_US_5w, $\overline{Cj}$ and decrease in dryer number are increased, as expected. Also, the energy ratio is increased because retrofitted cases have a higher energy ratio than the prior US module cases.
- When the prior US section's length is doubled, $\overline{Cj}$ and the decrease in dryer number are doubled without compromising the energy ratio. A similar conclusion can be made for the retrofitted US cases.

Proportions of thermal effects and US phenomena

In contrast to non-contact US, drying rate estimated by the direct-contact US contains the thermal effects of the transducer. To assess the overall contribution of the thermal load of the heated transducer to the experimental drying rate correlation ($J_{w,o}$), a numerical analysis is performed. First, the transducer's surface temperature is measured with an IR camera while there is no load on the US transducer. In **Fig. 7a**, the maximum temperature of the transducer is plotted with respect to the transducer's ON time. Then, drying of a moist paper was simulated when it was placed on a "regular" hot plate with a transient surface temperature of $T_{t,max}$. The same governing equations are used as Asensio and Seyed-Yagoobi [9] but with altered boundary conditions to capture the fixed temperature at the bottom and the natural convection and evaporation at the top surface with T_∞=19°C. The convective heat transfer is estimated by the natural convection correlations [33] of a horizontal isothermal surface.

The average temperature and DBMC of the moist paper placed on the hot plate are shown in Fig. 7b and Fig. 7c. As expected, the sample's average temperature follows a

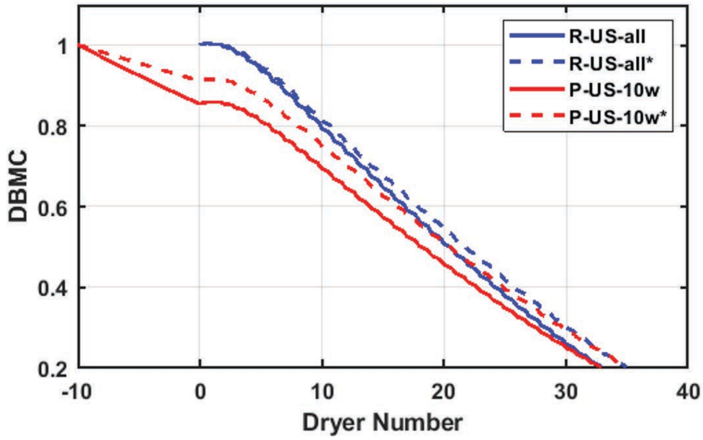

8. Numerical data: DBMC vs. dryer number for US cases with (solid line) and without (dashed line) thermal effect adjustment in the US liquid flux equation.

similar but delayed increase with time compared to the "hot plate" temperature. Figure 7d shows the vapor mass flux that exits the porous medium due to surface evaporation ($J_{v,o}$) at the top surface with respect to DBMC. From the initial DBMC of 1.5 to 1.25, during the initial heat-up period, the $J_{v,o}$ increases as expected. After that, $J_{v,o}$ monotonically declines because of the decrease in the moisture availability at the surface. On the same plot, the original liquid flux ($J_{w,o}$) correlation due to in-contact ultrasound was also plotted for comparison. By a rough estimation, the adjusted liquid flux $(J_{w,o})^*$ can be estimated by ($J_{w,o}$) – ($J_{v,o}$) to exclude the thermal effects. To compare the proportions of thermal effects and ultrasound mechanism, $(J_{w,o})'$ is divided by ($J_{w,o}$) and the resultant ratio is called mass flux ratio, as shown in Fig. 7e. The higher the mass flux ratio, the lower the thermal effects on the magnitude of the liquid flux. Overall, the mass flux ratio is around 0.6. Note that this estimation for thermal effects does not explain the possible attenuation of US due to the space between the paper sheet and the transducer when more practical non-contact US is used.

Retrofitted and prior US cases were simulated using the updated liquid flux, $(J_{w,o})^*$ and results are shown in **Fig. 8** and **Table V**. The $\overline{C}_j$ of new results (R_US_all* and P_US_10w*) are decreased because of the mitigated liquid flux values. However, both R_US_all* and P_US_10w* still show a 10% enhancement in drying compared to the baseline case. In addition, both cases' energy ratio deteriorates, because the drying performance becomes less effective with the same energy input. It is essential to mention that the paper experienced bulging (lift-off of paper while drying under no pressure) during the US experiments. Therefore, this analysis is an overprediction of the transducer's thermal effects.

CONCLUSIONS

To demonstrate the potential impact of an ultrasound (US) mechanism on paper drying, a numerical study was conducted to simulate a two-tiered configuration of the dryer section on a paper machine in the presence of installed US modules. A US drying rate correlation was used to represent the US drying and was obtained experimentally where the US transducers were in direct contact with the paper samples. A previously validated theoretical model of paper

Cases	Average Comparison Ratio ($\overline{C}j$), %	Decrease in Dryer Number, %	Energy Ratio
R_US_all	8.9	15.4	0.67
R_US_all*	5.4	10.3	0.39
P_US_10w	24.9	15.4	0.38
P_US_10w*	13.9	10.3	0.23
* Excluding thermal effects in the US drying rate correlation.			

V. The effect of US transducer thermal loads on the numerical model results for selected cases.

drying was adopted, and boundary conditions were adjusted to incorporate the effect of ultrasound using the US drying rate correlation. The US dryer modules were placed in the pockets and/or just upstream of the dryer drum section. It is important to mention that most of the conclusions related to dryers are based on the numerical model, and placing US modules into a paper machine could have some challenges. However, as a novel drying method, US needed to be explored in the field of paper drying to demonstrate the possible impact.

The average moisture content and temperature during drying, moisture removal rates by liquid (due to the US) and vapor forms, and total energy consumption were analyzed for all cases. Results show that the application of US decreases the total number of dryer drums for drying paper. For example, with US modules installed in every pocket, the total mass flux leaving the paper could be increased by up to ~9%, resulting in 15% fewer dryers required to remove the free water from the paper. This means that the paper's sheet speed can be increased for a given dryer number, and throughput can be increased. Furthermore, the scenario where the US modules are installed upstream of the dryer drum section has a much higher drying performance compared to the baseline case at the beginning of drying. Overall, retrofitted US cases seem to have a better drying performance and lower energy consumption than prior US cases. Also, US retrofitting may be a benefit for dryer-limited machines. In addition, thermal effects in the experimental US drying rate correlation were de-coupled or corrected. The corrected correlation was used to generate the effect of the thermal load of the transducer on the paper machine results. With the use of adjusted US correlation, the effect of US reduced to 10% from 15%.

As mentioned previously in this study, the US drying correlation was obtained with a US transducer in direct contact with the paper sample. Direct-contact US transducers are not applicable for a paper drying machine due to the possible breaking and tearing of paper. Thus, future work should apply ultrasound correlation obtained for a non-contact US transducer. In addition, the US drying rate should also be acquired for other types of fibers and other operating conditions, such as transducer load power and US frequency. **TJ**

ACKNOWLEDGEMENTS

This study was financially supported by the U.S. Department of Energy Office of Advanced Manufacturing under Award Number DE-EE0009125 and the Center for Advanced Research in Drying (CARD), a U.S. National Science Foundation Industry University Cooperative Research Center. CARD is located at Worcester Polytechnic Institute and the University of Illinois at Urbana-Champaign (co-site).

LITERATURE CITED

1. Statista, "Production volume of paper and cardboard worldwide from 2008 to 2018," Statista, Hamburg, 2020. Available [Online] https://www.statista.com/statistics/270314/production-of-paper-and-cardboard-in-selected-countries/ <25 Dec 2020>.
2. Shirkole, S.S. and Mujumdar, A.S., *Drying Technol.* 38(14): 1817(2020). https://doi.org/10.1080/07373937.2020.1822080.
3. Miller, T., Kramer, C., and Fisher, A., "Bandwidth study on energy use and potential energy saving opportunities in U.S. pulp and paper manufacturing," U.S. Department of Energy, Washington, DC, 2015.
4. Stenström, S., *Drying Technol.* 38(7): 825(2019). https://doi.org/10.1080/07373937.2019.1596949.
5. Mujumdar, A.S., *Handbook of Industrial Drying*, Dekker, New York, 1987.
6. Lu, T. and Shen, S., *Appl. Therm. Eng.* 27(8-9): 1248(2007). https://doi.org/10.1016/j.applthermaleng.2006.11.005.
7. Nissan, A. and Hansen, D., *AIChE J.* 6(4): 606(1960). https://doi.org/10.1002/aic.690060420.
8. Seyed-Yagoobi, J., Bell, D., and Asensio, M., *J. Heat Transfer* 114(2): 538(1992). https://doi.org/10.1115/1.2911313.
9. Asensio, M.C. and Seyed-Yagoobi, J., *J. Energy Resour. Technol.* 115(4): 291(1993). https://doi.org/10.1115/1.2906435.
10. Seyed-Yagoobi, J., Sikirica, S.J., and Counts, K.M., *Drying Technol.* 19(3-4): 639(2001). https://doi.org/10.1081/DRT-100103940.
11. Asensio, M. and Seyed-Yagoobi, J., *Tappi J.* 75(10): 203(1992).
12. Hoshi, Y., Kuno, H., Takeshita, K., et al., *J. Heat Transfer* 30(2): 77(2001). https://doi.org/10.1002/1523-1496(200103)30:2<77::AID-HTJ1>3.0.CO;2-3.
13. Sadeghi, M. and Douglas, W.M., "From tissue to linerboard: validation of a microscale simulator for single technique and hybrid dryers," *Proc. Int. Drying Symp., 14th*, Unicamp Publishing House, Sao Paulo, 2004.
14. Asensio, M.C., Seyed-Yagoobi, J., Lehtinen, J.A., et al., *Drying Technol.* 13(4): 945(1995). https://doi.org/10.1080/07373939508916992.
15. Sadeghi, M., "Modeling and simulation of transport phenomena in paper drying," Ph.D. thesis, McGill University, Montreal, 2003.
16. Whitaker, S., *Adv. Heat Transfer* 13: 119(1977). https://doi.org/10.1016/S0065-2717(08)70223-5.
17. Coumans, W., "Transport parameters and shrinkage in paper drying," in *Drying 94* (V. Rudolph and R.B. Keey, Eds.), Elsevier, Amsterdam, 1994.
18. Harrmann, M. and Schulz, S., *Drying Technol.* 8(4): 667(1990). https://doi.org/10.1080/07373939008959910.
19. Karlsson, M. and Stenström, S., *Drying Technol.* 23(1-2): 165(2005). https://doi.org/10.1081/DRT-200047951.
20. Peng, C., Ravi., S., Patel, V.K., et al., 125: 498(2017). https://doi.org/10.1016/j.energy.2017.02.138.
21. Zhang, Y. and Abatzoglou, N., *Chem. Eng. Res. Des.* 154: 21(2020). https://doi.org/10.1016/j.cherd.2019.11.025.
22. Patel, V.K., Reed, F.K., Kisner, R., et al., *J. Therm. Sci. Eng. Appl.* 11(2): 021008(2019). https://doi.org/10.1115/1.4041596.

23. Dupuis, E.D., Momen, A.M., Patel, V.K., et al., *Appl. Energy* 235: 451(2019). https://doi.org/10.1016/j.apenergy.2018.10.100.
24. Asensio, M.C., "Transport phenomena during drying of deformable, hygroscopic porous media: Fundamentals and applications," Ph.D. dissertation, Texas A&M University, College Station, TX, USA, 1999.
25. Nissan, A. and Kaye, W., *Tappi* 38(7): 385(1955).
26. Park, S., Venditti, R.A., Jameel, H., et al., *Carbohydr. Polym.* 66(1): 97(2006). https://doi.org/10.1016/j.carbpol.2006.02.026.
27. Maloney, T. and Paulapuro, H., *J. Pulp Pap. Sci.* 25(12): 430(1999).
28. Reardon, S., Davis, M., and Doe, P., *Drying Technol.* 17(4-5): 655(1999). https://doi.org/10.1080/07373939908917563.
29. Schneeberger, M., Leuk, P., Hirn, U., et al., "The heat of sorption in paper drying — an investigation of measurement methods and influence of pulp parameters," in *Advances in Pulp and Paper Research, Trans. XVth Fund. Res. Symp., Cambridge*, 2013 (S.J. I'Anson, Ed.), FRC, Manchester, 2018, pp. 469-492.
30. Kong, L., Hasanbeigi, A., and Price, L., *J. Cleaner Prod.* 122: 5(2016). https://doi.org/10.1016/j.jclepro.2015.12.116.
31. Rahnama Mobarakeh, M., Santos Silva, M., and Kienberger, T., *Energies* 14(4): 1161(2021). https://doi.org/10.3390/en14041161.
32. Patel, V.K., "Ultrasonic clothes dryer," U.S. Department of Energy Office of Energy Efficiency & Renewable Energy, Washington, DC, 2019. Available [Online] https://www.energy.gov/sites/default/files/2019/05/f62/bto-peer-2019-ornl-ultrasonic-clothes-dryer.pdf <08March2022>.
33. Incropera, F.P., DeWitt, D.P., Bergman, T.L., et al., *Principles of Heat and Mass Transfer*, 6th edn., John Wiley & Sons, Hoboken, NJ, 2006.

ABOUT THIS PAPER

Cite this article as:
Asar, M.E., Noori, Z., and Yagoobi, J., *TAPPI J.* 21(3): 127(2022). https://doi.org/10.32964/TJ21.3.127

DOI: https://doi.org/10.32964/TJ21.3.127

ISSN: 0734-1415

Publisher: TAPPI Press

About this journal

APPENDIX

The following is a list of terms used in this paper:

BW	Basis weight, kg/m^2
c	Specific heat, J/(kgK)
C_j	Comparison ratio; moisture removal rate by the liquid form/moisture removal rate by the vapor form
$\overline{C_j}$	Average comparison ratio
$DBMC$	Dry basis moisture content; weight of water/weight of dry fibers
$\overline{DBMC}$	Average DBMC across thickness direction
D_v	Vapor diffusivity, m^2/s
h_i	Interface thermal contact conductance, W/(m^{2}K)

ABOUT THE AUTHORS

Ultrasound (US)-assisted drying can be considered as a novel drying technology for the pulp and paper industry. Thus far, US drying has mainly been studied for fabric and food products. Therefore, there is a need for studies focusing on the application of the US mechanism within the drying section of a paper machine.

In this paper, for the first time, the effect of the application of a US mechanism in a multi-cylinder dryer section is investigated numerically. The most difficult aspect of this research was assessing the US drying mechanism compared to the baseline case.

It was interesting to find that for the operating conditions (experimental and numerical), the ultrasound's atomization requires more power to vibrate the liquid and generate liquid mist to escape from the paper than the baseline drying method.

Through our research, we found that ultrasound can increase the drying performance of a paper machine for mills. Also, retrofitted ultrasound modules can be a great fit for dryer-limited paper machines.

Asar

Noori

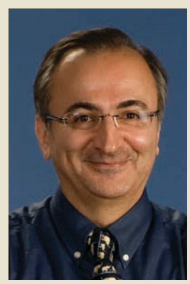

Yagoobi

This numerical study is based on the US correlation obtained with the US transducer in direct contact with the paper sample. Thus, future work should include US correlation based on a non-contact US transducer.

Asar is graduate research assistant; Noori is graduate research assistant; and Yagoobi is professor at the Center for Advanced Research in Drying, Multi-Scale Mass and Heat Transfer Laboratory, at Worcester Polytechnic Institute, Worcester, MA, USA. Email Asar at masar@wpi.edu.

H_{fg}	Enthalpy of vaporization of water, J/kg
k_m	Mass transfer coefficient, kg/(m²s)
η_{dryer}	Efficiency of multi-cylinder dryer section
$\eta_{transducer}$	Transducer efficiency
Δz	Step size or distance between two nodes, m
H	Enthalpy, J/kg
J	Mass flux, kg/(m²s)
K	Permeability, m²
k	Thermal conductivity, W/(m K)
M	Mass of liquid water in paper sheet, kg/m³
MW	Molecular weight, kg/kmol
P	Power, W/m²
P	Pressure, Pa
P_US	Prior US module/case where US modules are placed prior to the dryer drum section
PI-PIV	Phase I to IV of drying
q''	Heat flux, W/m²
R_US	Retrofitted US module/case
s	Saturation; volume of liquid/volume of voids
T	Temperature, K
t	Time, s
th	Thickness of paper sheet, m
US	Ultrasound
w	Length that is equivalent to the total length of Phases 1-4 for the selected dryer or 5.2 6m
WBMC	Wet basis moisture content; weight of water/total weight
y	Mole fraction
Z	Paper thickness, m
z	Axis across the thickness of paper sheet
ε	Porosity; volume of voids/total volume
ρ	Density, kg/m³

Superscript

$(\_)^*$	Excluding thermal effects or adjusted

Subscripts

a	Air
ap	Apparent
atm	Atmosphere
ca	Capillary
eff	Effective
f	Fiber
fin	Final (bone-dry)
init	Initial (inlet of dryer section)
max	Maximum
su	dryer surface
t	transducer
v	water vapor
v,o	water vapor to exterior
va	Vapor in air
w	Liquid water
w,o	Liquid water to exterior